*Remote Sens.* **2014**, *6*, 3170-3187; doi:10.3390/rs6043170

OPEN ACCESS

*remote sensing*

**ISSN 2072-4292**

www.mdpi.com/journal/remotesensing

*Article*

# Surface Soil Water Content Estimation from Thermal Remote Sensing based on the Temporal Variation of Land Surface Temperature

**Dianjun Zhang [1,2], Ronglin Tang [1,*], Wei Zhao [3], Bohui Tang [1], Hua Wu [1], Kun Shao [4] and Zhao-Liang Li [5]**

[1] Key Laboratory of Resources and Environmental information System, Institute of Geographic Sciences and Natural Resources Research, Chinese Academy of Sciences, Beijing 100101, China; E-Mails: zhangdianjun123@163.com (D.Z.); tangbh@igsnrr.ac.cn (B.T.); wuhua@igsnrr.ac.cn (H.W.)

[2] University of Chinese Academy of Sciences, Beijing 100049, China

[3] Institute of Mountain Hazards and Environment, Chinese Academy of Sciences, Chengdu 610041, China; E-Mail: zhaow@imde.ac.cn

[4] School of Computer and Information, Hefei University of Technology, Hefei 230009, China; E-Mail: shaokun@hfut.edu.cn

[5] Key Laboratory of Agri-Informatics, Ministry of Agriculture, Institute of Agricultural Resources and Regional Planning, Chinese Academy of Agricultural Sciences, Beijing 100081, China; E-Mail: lizhaoliang@caas.cn

* Author to whom correspondence should be addressed; E-Mail: trl_wd@163.com; Tel.: +86-10-6488-9277.

*Received: 19 December 2013; in revised form: 20 March 2014 / Accepted: 31 March 2014 / Published: 9 April 2014*

---

**Abstract:** Soil water content (SWC) is a crucial variable in the thermal infrared research and is the major control for land surface hydrological processes at the watershed scale. Estimating the surface SWC from remotely sensed data using the triangle method proposed by Price has been demonstrated in previous studies. In this study, a new soil moisture index (Temperature Rising Rate Vegetation Dryness Index—TRRVDI) is proposed based on a triangle constructed using the mid-morning land surface temperature (LST) rising rate and the vegetation index to estimate the regional SWC. The temperature at the dry edge of the triangle is determined by the surface energy balance principle. The temperature at the wet edge is assumed to be equal to the air temperature. The mid-morning land surface temperature rising rate is calculated using Meteosat Second Generation—Spinning

Enhanced Visible and Infrared Imager (MSG-SEVIRI) LST products over 4 cloud-free days (day of year: 206, 211, 212, 242) in 2007. The developed TRRVDI is validated by *in situ* measurements from 19 meteorological stations in Spain. The results indicate that the coefficient of determination ($R^2$) between the TRRVDI derived using the theoretical limiting edges and the *in situ* SWC measurements is greater than that derived using the observed limiting edges. The $R^2$ values are 0.46 and 0.32; respectively ($p < 0.05$). Additionally, the TRRVDI is much better than the soil moisture index that was developed using one-time LST and fractional vegetation cover (FVC) with the theoretically determined limiting edges.

**Keywords:** thermal infrared; soil water content; triangle method; TRRVDI; temperature rising rate

## 1. Introduction

Soil water content (SWC) is an important parameter in the study of hydrology, meteorology, agriculture management and global climate change [1–9]. It influences energy partitioning between sensible and latent heat fluxes, and the exchange of water and energy fluxes between the land surface and the atmosphere [9]. Additionally, the SWC is an indispensable variable in many hydrological and atmospheric processes.

The conventional method (such as the gravimetric method) is accurate but is destructive and time consuming to acquire [9]. Although the SWC can be estimated by Time Domain Reflectometry (TDR) or with the neutron attenuation method, these methods are in essence point based. Local scale variations in soil properties, terrain and vegetation cover make it difficult to select representative field sites [10]. Field methods are complex, labor-intensive and expensive. Remote sensing methods, however, can monitor a larger region and obtain images at short time intervals. For example, the geostationary meteorological satellites can provide 96 temporal series data in one day. Due to the advantages of remote sensing, many authors have tried to estimate the SWC estimation using this technique [11–14]. Optical remote sensing applies the reflectance (s) of different bands to obtain the SWC for different soils [15–17]. Thermal remote sensing uses soil thermal properties to study the soil moisture using methods such as the thermal inertia method or the triangle method [18–23]. Microwave remote sensing estimates the SWC using a passive radiometer or the relationship between the SWC and the backscattering coefficients from radar [24–28].

The surface temperature-vegetation index/fractional vegetation cover triangle method, which is easy to operate and requires less ground auxiliary data, is widely used in the SWC and evapotranspiration (ET) research [6,29–35]. Land surface temperature reflects the complicated effects of the soil properties and the incoming and outgoing energies. The vegetation index shows the complex conditions of the underlying surface. Many previous studies [36–38] utilize these two variables to study the SWC inversion through different remotely sensed data sources. The triangular space constructed by the LST and the vegetation index has been proven to be useful to monitor the SWC at a regional scale [9,39]. According to previous studies, land surface temperature and vegetation

index/fractional vegetation cover show a strongly negative relationship. The slope of the relationship is related to the sensible heat flux, evapotranspiration and the surface SWC. Additionally, the triangular space has also been used to estimate the crop temperature or air temperature, *etc.* [39].

The surface temperature-vegetation index triangle method assumes that there is a wide change of both land use cover from bare soil to the full vegetation cover and surface SWC from dry to wet conditions. One major limitation of the triangle method is the determination of the dry edge from the constructed space [32]. The dry edge in the triangular space indicates that the vegetation is subject to water stress, evapotranspiration reaches the minimum and the SWC is 0, meaning that no water can be used. Different approaches have been developed to reduce the errors from data resources and limiting edge extractions. The instantaneous land surface temperature and vegetation index are used to construct the triangular space [40–45]. The limiting edges are determined through the empirical fitting or from the physical equations. The surface SWC estimation results can be seriously affected by the error induced by the instantaneous land surface temperature retrievals, Land surface temperatures from different times are applied in the triangle method, and the soil moisture index is proposed. Determining the limiting edge of these methods, however, is all based on the observed scatter in the space without a physical basis [29,46]. A combination of the land surface temperature variations with the physical limiting edge determination method is therefore required. In this study, the land surface temperature time series variation is used to reduce the error induced by the instantaneously obtained values. The theoretical limiting edges are determined by the energy balance model with a robust physical basis to avoid the uncertainty caused by the observed limiting edges. The new soil moisture index, TRRVDI, is then proposed based on the land surface temperature time series variations and vegetation index with the theoretical limiting edge determination and is used to estimate the SWC in the study area.

The objectives of this research are as follows: (1) to develop a new soil moisture index based on the temporal variation of land surface temperatures in the mid-morning on a clear sky day; and (2) to validate the index using the *in situ* volumetric soil moisture content measurements and compare it to two other soil moisture indices. In Section 2, the TRRVDI is developed using the space that constructed by the land surface temperature mid-morning rising rate and the fractional vegetation cover. The limiting edges are determined by the energy balance model. MSG SEVIRI data, *in situ* measurements and the study area are described in Section 3. Section 4 illustrates the comparisons with the *in situ* measurements. The conclusions are presented in Section 5.

## 2. Method

### *2.1. Definition of the Temperature Rising Rate Vegetation Dryness Index (TRRVDI)*

In the triangular or trapezoidal space, the theoretical dry edge is characterized by zero evapotranspiration and water unavailability. The theoretical wet edge represents the surface over which there is enough water to allow evaporation to occur under unrestricted conditions and the vegetation is not stressed by the SWC. Because of the uptake water from the root zone by plants, the observed dry edge may not represent the real water-limiting conditions [9]. According to Sandholt [34], the land surface temperature (Ts) decreases with increasing surface SWC under a given vegetation cover and environmental conditions. In the triangle space, the pixel values are projected onto a two-dimensional

scatterplot represented by Ts on the y-axis and the vegetation index (VI) on the x-axis; and the variation in soil moisture is represented by the slope of the relationship between Ts and the VI. The soil water isopleths in the space are assumed to be linear lines from the maximum vegetation cover to the bare soil, and the soil water decreases linearly with the increase of Ts. The soil moisture index is defined as the ratio of the temperature of the intermediate pixel minus the minimum temperature to the maximum temperature minus the minimum temperature for a given vegetation index [34]. The maximum temperature is assumed to linearly relate to the vegetation coverage at the dry edge.

Because of the error induced by the instantaneous temperature obtained via remote sensing, many studies use the temperature difference to estimate the SWC. Moran [39] used the difference between the land surface temperature and the air temperature to study crop water deficit conditions. Using the difference between the maximum and minimum land surface temperatures, Stisen *et al.* [29] proposed that the land surface temperature difference in one day can be used to estimate the SWC. Polar-orbiting satellites, however, can only provide three or four images of a given site on a daily basis. When the weather is rainy or cloudy, the data are not available. Geostationary meteorological satellites are useful because they can provide data every 15 minutes. MSG data are widely used in soil water content and ET monitoring studies [29,47,48].

The mid-morning land surface temperature increases linearly on a sunny day [46]. The land surface temperature rising rate is related to the SWC on the sunny day. The temperature rising rate-vegetation index triangular or trapezoidal space is defined and shown in Figure 1. The vertical axis represents the mid-morning land surface temperature rising rate, and the horizontal axis represents the fractional vegetation cover. The theoretical dry edge indicates that the TRRVDI reaches its maximum value and is equal to 1. The theoretical wet edge indicates that the SWC is sufficient and that the TRRVDI is equal to 0. The assumptions are that the land surface temperature rising rate is lineally related to the fractional vegetation cover and that the soil water availability varies linearly from the dry edge to the wet edge.

**Figure 1.** An illustration of the Temperature Rising Rate Vegetation Dryness Index (TRRVDI). RT is the rate of land surface temperature in the mid-morning. RTsd and RTvd are the driest points for bare soil and full vegetation, respectively. RTsw and RTvw are the wettest points for bare soil and full vegetation, respectively. The red dotted line is the observed dry edge and the upper blue solid line is the theoretical dry edge derived from the energy balance equation. For a given pixel (C), CB and AB are used to calculate the TRRVDI.

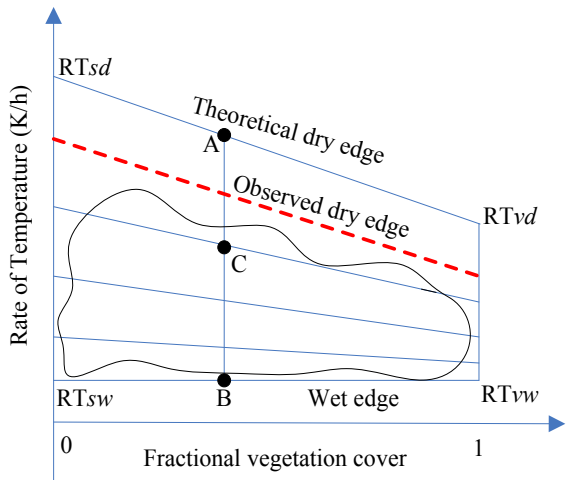

The soil moisture index TRRVDI is defined as:

$$TRRVDI = \frac{RT_{(i)} - RT_{wet}}{RT_{dry} - RT_{wet}} \quad (1)$$

where $RT_{(i)}$ is the mid-morning rising rate of the surface temperature for a pixel i, which is obtained by the temperature difference at 8:30 AM and 11:30 AM divided by the time difference. $RT_{wet}$ is the minimum RT in the triangle that defines the wet edge, and $RT_{dry}$ is the maximum RT at the dry edge.

Figure 1 shows that the theoretical limiting edges are different from the observed edges. Numerous methods are developed from different starting points. Moran [39] determined the dry edge from the theoretical boundary lines of the difference between the land surface temperature and air temperature. Sandhlot [34] used the observed dry edge from the scatter plot derived from the remotely sensed data directly. Tang *et al.* [35,49] developed the dry edge auto-determined method from the scatterplots, and this method has been widely used to estimate the evapotranspiration. Zhang proposed a theoretical method to determine the dry edge using the energy balance equation for evapotranspiration [50,51]. His method demonstrated that the theoretical boundary line is different from the observed one. The observed dry edge is generally not the soil moisture content associated with the wilting point of the soil or evapotranspiration that is equal to 0, which means that the observed dry edge is not the true dry edge. The dry edge represents a condition in which no water is available to evaporate and the SWC is zero. The land surface is at its driest condition when the land surface temperature reaches its maximum value, which is associated with stomatal closure in the vegetated area. In particular, the stomata close completely for the vegetated area. Similarly, the wet edge is represented by the minimum land surface temperature associated with a non-restricting SWC [52]. In general, the observed dry edge from the scatterplot of remote sensing data is not the theoretical dry edge. The vegetated area does not typically reach the driest condition because the plants can continue to obtain water from deeper in the root zone. In this paper, the theoretical limiting edges are determined using the method discussed by Zhang [51].

### *2.2. The Theoretical Dry Edge Determination*

The land surface energy balance equation is

$$Rn = LE + G + H \quad (2)$$

where $Rn$ is the surface net radiation, LE is the latent heat flux, G is the soil heat flux and H is the sensible heat flux. Rn can be expressed as

$$Rn = S_0(1-\alpha) + \varepsilon_s \sigma \varepsilon_a T_{sa}^4 - \sigma \varepsilon_s T_s^4 \quad (3)$$

where $S_0$ is the solar radiation reaching the Earth's surface, *á* is the albedo, *ó* is Stefan-Boltzmann constant. $T_{sa}$ is the average sky temperature and $T_s$ is the land surface temperature. $å_a$ is the atmospheric emissivity, which can be obtained by [51]

$$\varepsilon_a = 1.24(\frac{e_a}{T_a})^{1/7} \quad (4)$$

where $e_a$ is the water vapor pressure at a reference height and $å_s$ is the emissivity of the land surface, which can be given by [53].

$$\varepsilon_s = Fv\varepsilon_v + (1 - Fv)\varepsilon_{ss} \tag{5}$$

where $å_v$ and $å_{ss}$ are the emissivity for vegetation (0.97) and soil (0.95) respectively [53], and $F_v$ is the fractional vegetation cover. The soil heat flux can be estimated using [51]

$$G = Rn(\Gamma v + (\Gamma s - \Gamma v)(1 - Fv)) \tag{6}$$

where $Ãs$ and $Ãv$ are the ratios of $G$ and Rn for bare soil and a fully covered vegetation surface, respectively. The value of $Ãv$ is 0.05, and the value of $Ãs$ is 0.315. The vegetation cover is equal 0 for the dry bare soil.

When the soil reaches extreme dry conditions, there is no LE. The energy balance equation, therefore, can be shown as

$$Rn = G + H \tag{7}$$

The sensible heat flux can be calculated by the following aerodynamic equation [54]

$$H = \frac{\rho Cp(Ts - Ta)}{r_a} \tag{8}$$

where $ñ$ is the density of air and $Cp$ is the heat capacity of air at a constant pressure. $Ta$ is the air temperature and $r_a$ is the aerodynamic resistance.

Combining the above equations, $T_{sd}$ and $T_{vd}$ [51] are determined by

$$T_{sd} = \frac{0.7(S_0(1-\alpha_{sd}) + \sigma\varepsilon_a T_{sa}^4) + \dfrac{\rho Cp}{r_{sda}} T_{sda}}{\dfrac{\rho Cp}{r_{sda}} + 0.685\sigma\varepsilon_{soil} T_{sda}^3} \tag{9}$$

$$T_{vd} = \frac{0.7(S_0(1-\alpha_{vd}) + \sigma\varepsilon_a T_{sa}^4) + \dfrac{\rho Cp}{r_{vda}} T_{vda}}{\dfrac{\rho Cp}{r_{vda}} + 0.95\sigma\varepsilon_{veg} T_{vda}^3} \tag{10}$$

where the subscripts sd and vd denote the bare soil and full vegetation cover, respectively. The other parameters were previously explained. If the parameters $\alpha_{sd}$, $\alpha_{vd}$, $T_{sky}$, $r_{sda}$, $r_{vda}$, $T_{sda}$ and $T_{vda}$ are acquired, $T_{sd}$ or $T_{vd}$ can be iteratively calculated.

## 3. Study Area and Data

### *3.1. Study Area*

Considering the requirement of clear sky conditions, the central part of Spain was selected as the study area (238 pixels times 350 pixels with a spatial resolution of 3 km, as shown in Figure 2). The elevation in most of this region is greater than 450 m. For this study, regions with an elevation between 450 and 900 m were selected to minimize the effect of elevation changes on the surface temperature change. The main land cover type in this region is closed shrub lands and croplands.

**Figure 2.** DEM and experiment stations in the study area.

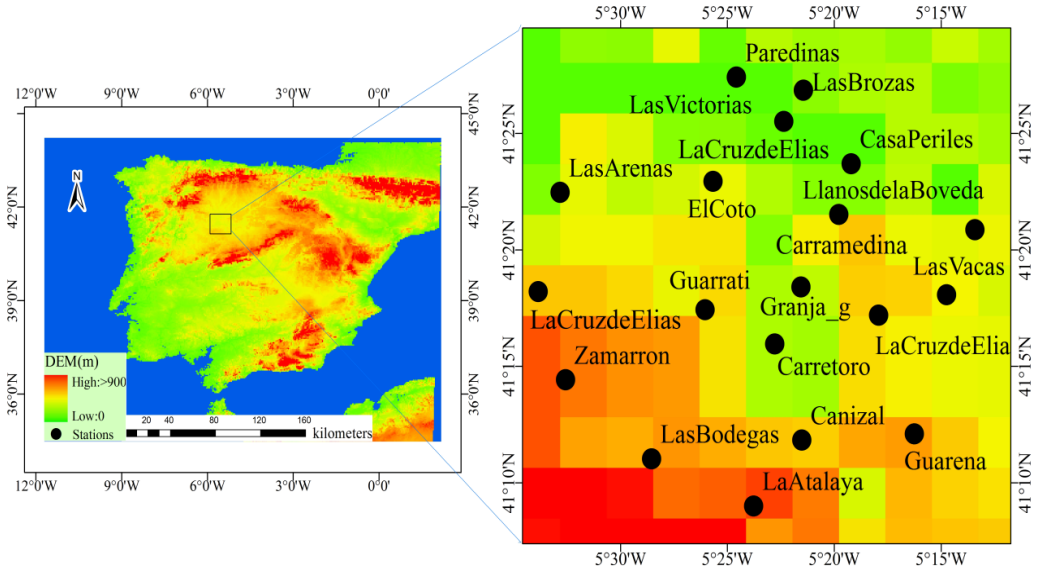


*3.2. Data*

3.2.1. MSG SEVIRI Data

As for satellite data, MSG-SEVIRI data is selected. The SEVIRI onboard the Meteosat Second Generation (MSG) satellite is a new type of geostationary sensor and includes a red and a near-infrared channel and two thermal infrared split window channels with 15-min acquisition intervals (Table 1). Its high temporal resolution and capability to provide 96 data in one day are advantageous, but its low spatial resolution of 4.8 km at nadir and large view angles are disadvantages. In this study, SEVIRI LST and fraction vegetation cover data downloaded from the Land Surface Analysis Satellite Applications Facility were used to derive the LST mid-morning rising rates and construct the feature space [55].

3.2.2. *In situ* Measurements

REMEDHUS is an important part of the International Soil Moisture Network [56] and has been used to validate several satellite products. REMEDHUS is composed of 20 soil moisture monitoring stations located in the Duero basin of Spain. The stations continuously measure the soil moisture at depths of 0-5 cm using Hydra probes (Stevens® Water Monitoring System, Inc., Oregon, USA). There are four automatic weather stations and several other sensors and equipment for hydrological monitoring. These stations are located within an area of 1300 km$^2$ (41.1° to 41.5°N; 5.1° to 5.7°W) in a central semiarid sector of the Duero basin that is nearly flat (less than 10% slope), with the elevation ranging from 700 to 900 m above sea level. It is a continental semiarid Mediterranean climate that has an average annual precipitation of 385 mm and a mean temperature of 12 °C. The land use is mainly agricultural, with rain-fed cereals grown in winter and spring (78%), irrigated crops in summer (5%), and vineyards (3%). There are also patchy areas of forest and pasture (13%). The growing cycle for rainfed cereals consists of the seeding period in autumn, development in spring and ripening/harvesting in early summer. The stations contain different soil types such as silty loam, loamy

sand and loam. The stations collect instantaneous (averaged over a 1-hour interval) *in situ* volumetric SWC at 5 cm depth concurrent with the satellite overpass times, as shown in Table 2.

**Table 1.** Spectral channel characteristics of MSG-SEVIRI [57]

| Channel No. | Channel Name | Characteristics of Spectral Channel (μm) | | | Short-Term Radiometric Error Performances | Main Gaseous Absorber or Window |
|---|---|---|---|---|---|---|
| | | $\lambda_{central}$ | $\lambda_{min}$ | $\lambda_{max}$ | | |
| 1 | VIS0.6 | 0.635 | 0.56 | 0.71 | 0.27 at 5.3 W/(m$^2$ sr μm) | Window |
| 2 | VIS0.8 | 0.81 | 0.74 | 0.88 | 0.21 at 3.6 W/(m$^2$ sr μm) | window |
| 3 | NIR1.6 | 1.64 | 1.50 | 1.78 | 0.07 at 0.75 W/(m$^2$ sr μm) | window |
| 4 | IR3.9 | 3.9 | 3.48 | 4.36 | 0.17 K at 300 K | Window |
| 5 | WV6.2 | 6.25 | 5.35 | 7.15 | 0.21 K at 250 K | Water vapor |
| 6 | WV7.3 | 7.35 | 6.85 | 7.85 | 0.12 K at 250 K | Water vapor |
| 7 | IR8.7 | 8.7 | 8.3 | 9.1 | 0.10 K at 300 K | Window |
| 8 | IR9.7 | 9.66 | 9.38 | 9.94 | 0.29 K at 255 K | Ozone |
| 9 | IR10.8 | 10.8 | 9.80 | 11.80 | 0.11 K at 300 K | Window |
| 10 | IR12.00 | 12.00 | 11.00 | 13.00 | 0.15 K at 300 K | Window |
| 11 | IR13.4 | 13.4 | 12.40 | 14.40 | 0.15 K at 300 K | Carbon dioxide |
| 12 | HRV | Broad channel (0.4–1.1 μm) | | | 0.63 at 1.3 W/(m$^2$ sr μm) | Window/Water vapor |

**Table 2.** Locations of the experiment stations and *in situ* volumetric soil moisture content at 19 stations concurrent with the satellite overpasses (day of year: 206, 211, 212 and 242) involved in this study.

| Station | Latitude | Longitude | *In situ* Volumetric Soil Moisture Content (m$^3$/m$^3$) at 5 cm Depth | | | |
|---|---|---|---|---|---|---|
| | | | 206 | 211 | 212 | 242 |
| Canizal | 41.19720°N | 5.35861°W | 0.24 | 0.21 | 0.24 | 0.19 |
| Carramedina | 41.31359°N | 5.16005°W | 0.30 | 0.23 | 0.22 | 0.31 |
| Carretoro | 41.26611°N | 5.37972°W | 0.28 | 0.10 | 0.29 | 0.25 |
| CasaPeriles | 41.39508°N | 5.32010°W | 0.29 | 0.19 | 0.30 | 0.13 |
| ConcejodelMonte | 41.30126°N | 5.24569°W | 0.21 | 0.15 | 0.14 | 0.27 |
| ElCoto | 41.38251°N | 5.42786°W | 0.33 | 0.19 | 0.34 | 0.25 |
| Granja_g | 41.30690°N | 5.35925°W | 0.21 | 0.12 | 0.25 | 0.27 |
| Guarena | 41.20170°N | 5.27085°W | 0.13 | 0.15 | 0.12 | 0.15 |
| Guarrati | 41.29050°N | 5.43402°W | 0.15 | 0.14 | 0.14 | 0.18 |
| LaAtalaya | 41.15011°N | 5.39621°W | 0.29 | 0.30 | 0.15 | 0.22 |
| LaCruzdeElias | 41.28662°N | 5.29868°W | 0.11 | 0.11 | 0.11 | 0.18 |
| LasArenas | 41.37455°N | 5.54714°W | 0.10 | 0.16 | 0.10 | 0.19 |
| LasBodegas | 41.18381°N | 5.47572°W | 0.14 | 0.22 | 0.11 | 0.17 |
| LasBrozas | 41.44765°N | 5.35734°W | 0.12 | 0.16 | 0.33 | 0.11 |
| LasVacas | 41.34778°N | 5.22361°W | 0.17 | 0.27 | 0.32 | 0.23 |
| LasVictorias | 41.42529°N | 5.37267°W | 0.27 | 0.18 | 0.28 | 0.14 |
| LlanosdelaBoveda | 41.35873°N | 5.32977°W | 0.14 | 0.19 | 0.10 | 0.18 |
| Paredinas | 41.45703°N | 5.40964°W | 0.31 | 0.24 | 0.31 | 0.22 |
| Zamarron | 41.24040°N | 5.54291°W | 0.28 | 0.29 | 0.12 | 0.20 |

## 4. Results and Discussion

### *4.1. Theoretical Dry Edge Determination and TRRVDI Results*

#### 4.1.1. The space of RT—Fractional Vegetation Cover (FVC)

The mid-morning temperature rising rate was calculated using MSG-SEVIRI LST for 4 cloud-free days (day of year (DOY): 206, 211, 212, 242) in 2007. The temperature rising rate—FVC space is plotted in Figure 3. A trapezoidal space can be observed from the temperature rising rate—FVC scatter. The temperature rate decreases when the vegetation cover increases. The temperature rising rate—FVC space changes from one value to another because of the variation of surface soil moisture content.

We can see that most of the rising rate of temperatures (RTs) changes from 2.0 to 8.0 K/h. When the soil is at its driest, the RT reaches its maximum of approximately 8.0 K/h, while the RT is approximately 4.0 K/h with a full vegetation cover. The spatial variation of RTs in the space is because that the leaf temperature of vegetation increased more slowly than did the bare soil at the same time interval. Assuming constant atmospheric conditions for a given day, the soil water content is the main factor in determining the RT changes. The RT changed largely on different days because the soil water content and atmospheric force varied greatly.

#### 4.1.2. The Theoretical Dry Edge Determination

Using the theories of Zhang *et al.* and Long *et al.* [51,52], the theoretical limiting edges of four images were determined (Figure 3). When the dry edge was calculated, the meteorological data from REMEDHUS were used. The air temperature, wind speed and downward longwave radiation were obtained from the station to calculate the RT at 8:30 and 11:30 AM. The dry points for bare soil and full vegetation cover were acquired physically to construct the theoretical dry edge. Based on the assumption that the temperature of the full vegetation cover was equal to the ambient air temperature, the theoretical wet edge was determined from the air temperature.

The theoretical dry edges on the four days are listed in Table 3 (X represents FVC and Y represents RT). The intercepts of the theoretical dry edges are larger, and the slope is smaller than the observed dry edges. The intercept of the dry edge shows the feasible maximum RT for one day, and the slope represents the soil moisture variation rate with fractional vegetation cover. It is shown that the observed dry edge fits well with the scatters, but the observed wet edge cannot fit well because of many outliers (pixels contaminated by cloud or located at a water body) in Figure 3. The theoretical limiting edges are close to the real conditions because many underlying surface measured data were used to derive them.

### *4.2. Comparisons*

To validate the TRRVDI, three soil moisture indices were used to compare to the *in situ* SWC at 19 stations. The first one was derived from the instantaneous land surface temperature and vegetation index with the theoretical limiting edges determination (ITVX) [34]. The second one was calculated from the land surface temperature rising rate and vegetation index with the observed

limiting edges from the scatterplots (TDX) [46]. The third one was the TRRVDI. The soil moisture indices ITVX and TDX are calculated as follows:

$$ITVX = \frac{LST_i - LST_{\min}}{LST_{\max} - LST_{\min}} \tag{11}$$

$$TDX = \frac{TD_i - TD_{\min}}{TD_{\max} - TD_{\min}} \tag{12}$$

where $LST_{\min}$ and $LST_{\max}$ are the minimum and maximum land surface temperature derived from the theoretical limiting edges, respectively. $LST_i$ is the instantaneous land surface temperature for a specific pixel. $TD_{\min}$ and $TD_{\max}$ are the minimum and maximum mid-morning land surface temperature difference derived from the observed limiting edges, respectively, and $TD_i$ is the mid-morning land surface temperature difference for a specific pixel.

**Figure 3.** The theoretical limiting edges determined from the energy balance equation and the observed dry and wet edges determined using the method proposed by Tang *et al.* [49] on 4 clear-sky images (day of year: 206, 211, 212 and 242).

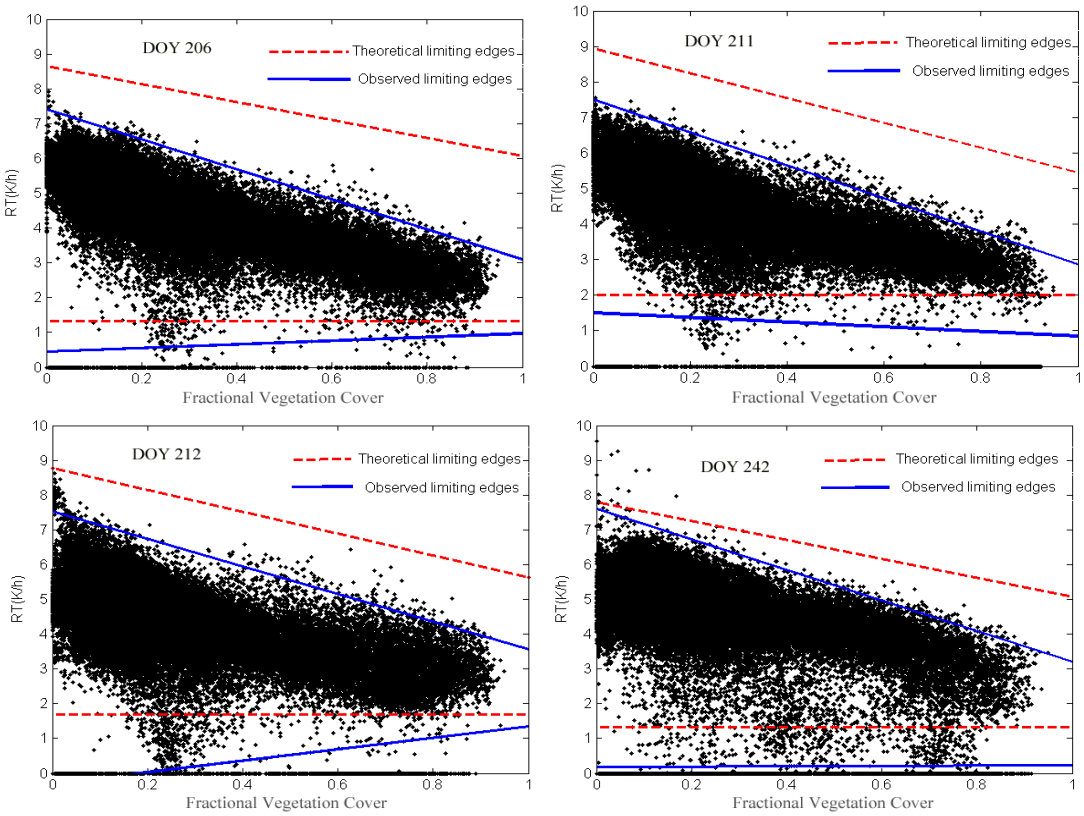


4.2.1. Comparison between the Theoretical and Observed Limiting Edges

Applying the method proposed by Tang *et al.* [49], the limiting edges determined by the regression of the scatter plot from the remotely sensed data are shown in Figure 3 (the blue line). The method used the spatial distribution of the scatters. The FVC is first divided into several small intervals, and the maximum land surface temperature in each interval is identified. The maximum pixels are then regressed as a line as the observed dry edge. The derivation of the wet edge is similar to that of the dry edge. The value of the observed dry edge is smaller than that of the theoretical one. The main reason

for this difference is that zero evaporation rarely occurs, as plants are able to extract water deeper in the root zone. Because of the weather effect on the soil moisture, the observed limiting edges are not the real extreme conditions of the land surface.

**Table 3.** Comparison of the theoretical and observed values for the dry edges for four sunny days in Figure 3 (X and Y represent the fractional vegetation cover and RT, respectively).

| Day of Year | Theoretical Dry Edge | Observed Dry Edge |
|---|---|---|
| 206 | $Y = 8.64 - 2.57X$ | $Y = 7.4 - 4.3X$ |
| 211 | $Y = 8.94 - 3.49X$ | $Y = 7.5 - 4.64X$ |
| 212 | $Y = 8.78 - 3.14X$ | $Y = 7.54 - 3.97X$ |
| 242 | $Y = 7.79 - 2.72X$ | $Y = 7.6 - 4.4X$ |

**Figure 4.** Comparison between the Temperature Rising Rate Vegetation Dryness Index (TRRVDI) and the soil moisture index derived from the land surface temperature rising rate and vegetation index with the observed limiting edges from the scatterplots (TDX). *p* value represents the statistical confidence level. The Relative Bias is calculated by the arithmetic mean of the difference of the two indices divided by the sample numbers.

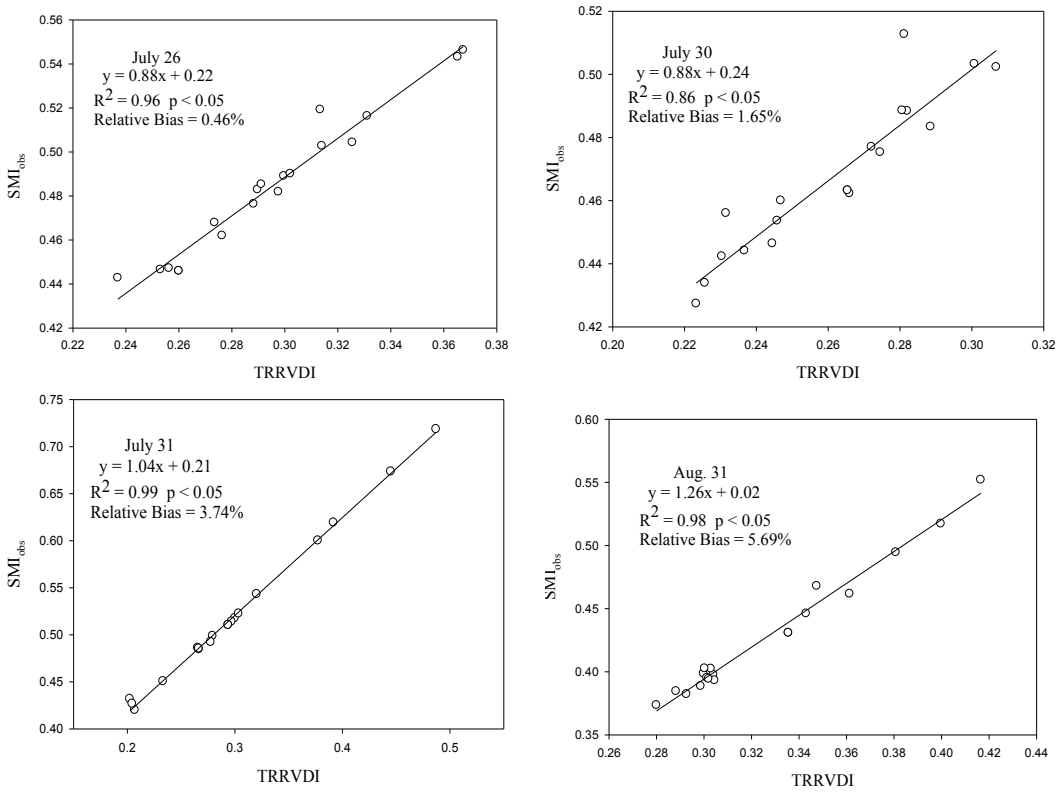


The soil moisture index derived from the theoretical limiting edges is smaller than the TDX, and the relationship between them is shown in Figure 4. The coefficients of determination between them are very high, demonstrating that the two soil indices are highly related. The coefficient of determination ($R^2$) can be greater than 0.86 ($p < 0.05$) and can even be as high as 0.99 ($p < 0.05$). Zhao [46] noted that the TDX is validated using the AMSR-E soil moisture products and API. The results demonstrated

that TDX can be used to monitor soil moisture variation and that it is suitable for monitoring the regional surface soil moisture and temporal variation [46]. The TRRVDI can therefore reflect drought conditions to a certain extent.

4.2.2. Comparison with *in situ* Measurements

Through the comparison of three soil moisture indices with the *in situ* SWC (Figure 5), the average $R^2$ of TRRVDI with *in situ* SWC can reach 0.46 ($p < 0.05$), and the other two are 0.32 ($p < 0.05$) and 0.36 ($p < 0.05$), respectively [58] (as shown in Table 4). The results show that TRRVDI is better than the other two indices at monitoring the soil water conditions. The coefficients varied over different days because of changing atmospheric conditions and the heterogeneity of the land surface. On DOY 211 and DOY 242, the TRRVDI was much better than the other two indices. The correlation coefficients demonstrated that the TRRVDI had a close relationship with the soil drought conditions. Based on the values of three soil moisture indexes, the TRRVDI was more indicative of the true land surface conditions. The TDX overestimated the SWC, which were different from the true drought conditions.

**Figure 5.** Comparison of the three different soil moisture indices with the *in situ* measurements soil water contents. The TDX represents the soil moisture index derived from the land surface temperature differences—vegetation index triangular space with the observed limiting edges; The ITVX shows the soil moisture index that derived from the instantaneous land surface temperature—vegetation index triangular space with the theoretical limiting edges. The TRRVDI is the soil moisture index proposed in this paper.

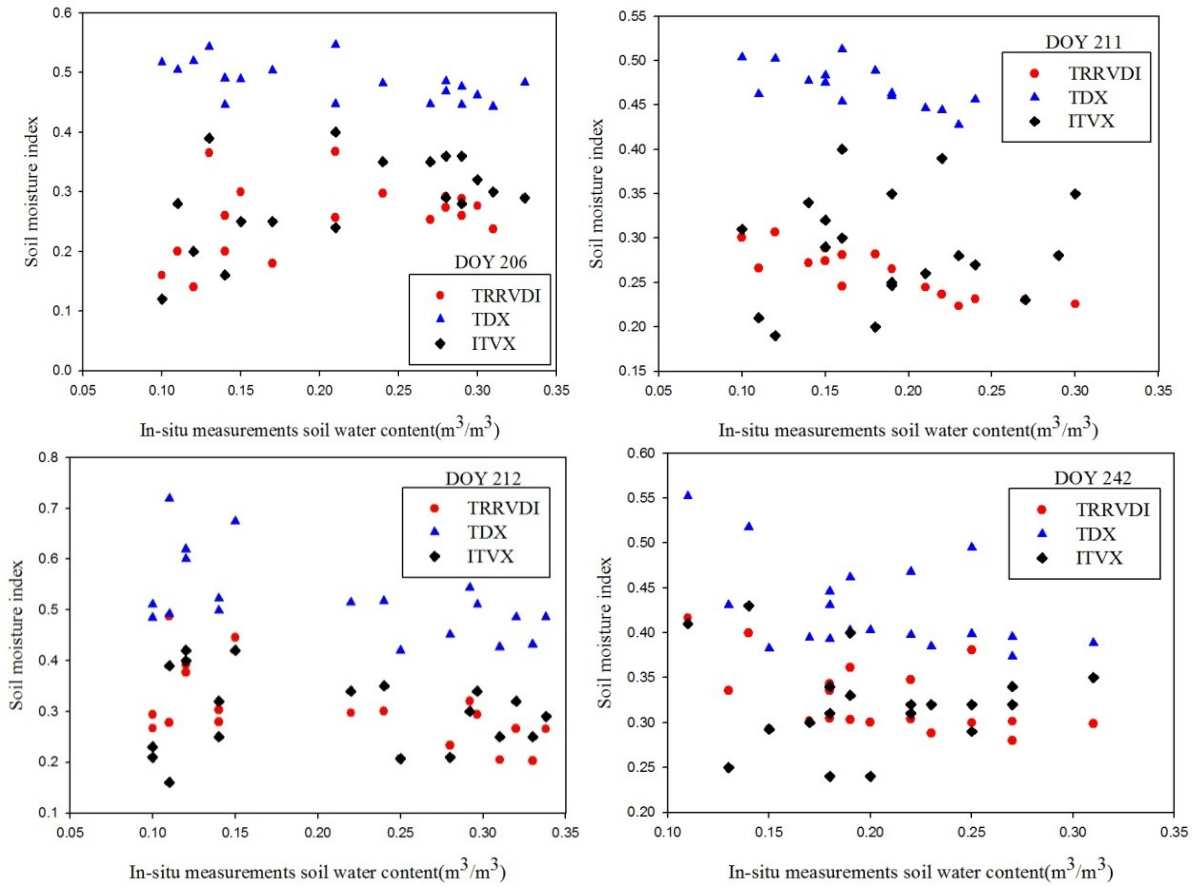

**Table 4.** Comparison of the three soil moisture indices with the *in situ* measurements soil water content for 4 sunny days (x and y represent the *in situ* volumetric soil water content and the soil moisture index, respectively). The TRRVDI is the Temperature Rising Rate Vegetation Dryness Index proposed in this paper, TDX is the soil moisture index derived from the land surface temperature rising rate and vegetation index with the observed limiting edges from the scatterplots and ITVX is the soil moisture index derived from the instantaneous land surface temperature and vegetation index with the theoretical limiting edges determination.

| Moisture Indexes | Day of Year | | | | $R^2$ | Relative Error |
|---|---|---|---|---|---|---|
| | 206 | 211 | 212 | 242 | | |
| TRRVDI | y = −1.25x + 0.58 | y = −1.54x + 0.59 | v = −0.67x + 0.41 | v = −0.92x + 0.50 | 0.46 | 4% |
| TDX | y = −1.37x + 0.88 | y = −1.38x + 0.84 | v = −0.62x + 0.53 | v = −0.60x + 0.46 | 0.32 | 11% |
| ITVX | y = −1.56x + 1.64 | y = −1.52x + 0.67 | v = −0.75x + 0.82 | v = −0.80x + 0.72 | 0.36 | 9% |

### *4.3. Discussions*

Compared with the soil moisture index derived from the observed limiting edges, the $R^2$ between the TRRVDI with the theoretical limiting edges is slightly improved, but it is still low, especially on DOY 206 and DOY 212. There are many reasons for the error, such as a scale mismatch, theoretical dry edge determination limitations or input data errors.

The validation data are obtained from meteorological stations that only represent the limited space around the stations or several meters away from the stations. However, the remote sensing pixel has an approximately ~3 kilometer spatial coverage of the land surface. A pixel is the complex information of the underlying surface that contains many land covers. Errors are induced by using point data to validate the estimated results. The spatial variation can't be precisely conveyed through the point data validation.

Monitoring soil moisture based on the space of Ts–FVC assumes that the meteorological parameters and land surface attributes are homogeneous, which simplifies the relationship between soil moisture and land surface temperatures [53]. In the study area, the land cover is not from bare soil to full vegetation cover. Additionally, in determining the theoretical dry edge, many assumptions can induce uncertainties. Among them, the aerodynamic resistance affects the results through the theoretical dry point for bare soil and full vegetation cover. The theoretical wet edge is determined by the air temperature, which can overestimate the true temperature of the wet edge. The results can be improved if the surface temperature of a water body is chosen as the theoretical wet edge.

In addition, the meteorological data used to obtain the theoretical dry edge may not represent the conditions corresponding to the maximum land surface temperature for bare soil or full vegetation cover. Determining the theoretical dry edge, however, is based on the observed values. If the observed dry conditions are not close to the real surface dry conditions, errors can be introduced.

## 5. Conclusions

Surface soil water content is of great importance in closing hydrologic budgets, assessing soil plant water interactions and studying climate change. This study developed a new soil water content index

using land surface temperature time series data to monitor the soil moisture conditions in combination with the Meteosat Second Generation—Spinning Enhanced Visible and Infrared Imager (MSG-SEVIRI) data. The mid-morning land surface temperature rising rate and vegetation cover were constructed to take on a trapezoidal space. The theoretical limiting edge determination method of Zhang [51] was used to derive the limiting edges. The greatest advantage of Temperature Rising Rate Vegetation Dryness Index (TRRVDI) is that it substitutes the temporal variation of land surface temperature (LST) for the instantaneous LST, which may reduce uncertainties in estimating the soil moisture. Additionally, based on the energy balance model, the determined TRRVDI has a robust physical basis and assumes that the soil water content changes linearly with the land surface temperature rising rate from bare soil to the full vegetation cover. The limitation is that the theoretical dry edge determination still needs auxiliary measured data. The basic conclusions are as follows:

(1) The TRRVDI is obtained using the temporal variation of LST rather than the instantaneous LST and the vegetation cover with the theoretical dry edge determination. The proposed soil moisture is more robust than those determined by the observed limiting edges. Many atmospheric parameters are incorporated into the energy balance equation to strengthen the accuracy of calculating the maximum dry point in the scatters.

(2) Compared with the *in situ* measurements, the TRRVDI is more robust than the two other soil moisture indices. The average $R^2$ of the TRRVDI (0.46, $p < 0.05$) is greater than that of the other two indices (0.32 and 0.36, $p < 0.05$). Additionally, the relative error of TRRVDI (4%) is lower than that of the other two indices (11% and 9%). The results demonstrated that the proposed soil moisture index is better than the other two indices for monitoring regional drought conditions.

We acknowledge that the soil moisture monitored in the upper 5 cm or less is of limited use for hydrologic and agricultural applications, which is primarily constrained by remote sensing. The greatest advantage of remote sensing is its ability to spatially continuously monitor large areas, which cannot occur with a limited number of ground-based stations. If the vertical soil moisture profile can be known a priori, one can extrapolate the remote sensing based soil moisture in the upper soil to the deep layer. Difficulties in applying the TRRVDI include the need for many ground auxiliary data and the complicated calculation processes. The index also requires different atmospheric forcing data to obtain the dry edge for different days. The energy closure and the complexity of the land surface lead to great uncertainties. To accurately monitor soil water conditions, further validations are required to assess the validity and utility of the TRRVDI.

## Acknowledgments

The work described in this publication has been supported by the Exploratory Forefront Project for the Strategic Science Plan in IGSNRR, CAS under grant 2012QY006, and supported in part by the National Nature Science Foundation of China under Grant No. 41201366, 41101332 and 41162011.

## Author Contributions

Dianjun Zhang wrote the manuscript with the contributions from all co-authors and was responsible for the research design, data preparation and analysis. Ronglin Tang and Zhao-Liang Li conceived and

designed the research. Wei Zhao, Bohui Tang, Hua Wu and Kun Shao collected and analyzed the *in situ* measurement data and performed the remotely sensed data processing.

## Conflicts of Interest

The authors declare no conflict of interest.

## References

1. Jackson, T.J.; Hawley, M.E.; O'Neill, P.E. Preplanting soil moisture using passive microwave sensors. *Water Resour. Bull*. **1987**, *23*, 11–19.
2. Pardé, M.; Zribi, M.; Wigneron, J.P.; Dechambre, M.; Fanise, P.; Kerr, Y.; Crapeau, M.; Saleh, K.; Calvet, J.C.; Albergel, C.; *et al.* Soil moisture estimations based on airborne CAROLS L-Band microwave data. *Remote Sens*. **2011**, *3*, 2591–2604.
3. Topp, G.C.; Davis, J.L.; Annan, A.P. Electromagnetic determination of soil water content: Measurements in coaxial transmission lines. *Water Resour. Res.***1980**, *16*, 574–582.
4. Fast, J.D.; McCorcle, M.D. The effect of heterogenous soil moisture on a summer baroclinic circulation in the central United States. *Mon. Wea. Rev.* **1991**, *119*, 2140–2167.
5. Long, D.; Singh, V.P. A two-source trapezoid model for evapotranspiration (TTME) from satellite imagery. *Remote Sens. Environ.* **2012**, *121*, 370–388.
6. Tang, R.L.; Li, Z.-L.; Jia, Y.; Li, C.; Sun, X.; Kustas, W.P.; Anderson, M.C. An intercomparison of three remote sensing-based energy balance models using Large Aperture Scintillometer measurements over a wheat-corn production region. *Remote Sens. Environ.* **2011**, *115*, 3187–3202.
7. Li, Z.-L.; Tang, B.H.; Wu, H.; Ren, H.; Yan, G.; Wan, Z. Satellite-derived land surface temperature: Current status and perspectives. *Remote Sens. Environ.* **2013**, *131*, 14–37.
8. Saha, S.K. Assesment of regional soil moisture conditions by coupling satellite sensor data with a soil-plant system heat and moisture balance model. *Int. J. Remote. Sens.* **1995***.16*, 973–980.
9. Wang, L.L. Satellite remote sensing applications for surface soil moisture monitoring: A review. *Front. Earth Sci.* **2009**, *3*, 237–247.
10. Verstraeten, W.W.; Veroustraete, F.; van der Sande, C.J.; Grootaers, I.; Feyen, J. Soil moisture retrieval using thermal inertia, determined with visible and thermal spaceborne data, validated for European forests. *Remote Sens. Environ.* **2006**, *101*, 299–314.
11. Liu, W.D.; Baret, F.; Gu, X.F.; Tong, Q.X.; Zheng, L.; Zhang, B. Relating soil surface moisture to reflectance. *Remote Sens. Environ.* **2002**, *81*, 238–246.
12. Price, J.C. On the analysis of thermal infrared imagery: The limited utility of apparent thermal inertia. *Remote Sens. Environ.* **1985**, *18*, 59–73.
13. Goward, S.N., Xue, Y.; Czajkowski, K.P. Evaluating land surface moisture conditions from the remotely sensed temperature/vegetation index measurements: An exploration with the simplified simple biosphere model. *Remote Sens. Environ.* **2002**, *79*, 225–242.
14. Li, Z.-L.; Wu, H.; Wang, N.; Qiu, S.; Sobrino, J.A.; Wan, Z.; Tang, B.H.; Yan, G. Land surface emissivity retrieval from satellite data. *Int. J. Remote Sens.* **2013**, *34*, 3084–3127.

15. Whiting, M.L.; Li, L.; Ustin, S.L. Predicting water content using Gaussian Model on soil spectra. *Remote Sens. Environ*. **2004**, *89*, 535–552.
16. Idso, S.B.; Schmugge, T.J.; Jackson, R.D.; Reginato, R.J. The utility of surface temperature measurements for the remote sensing of surface soil water status. *J. Geophys. Res.* **1975**, *80*, 3044–3049.
17. Idso, S.B.; Jackson, R.D.; Reginato, R.J.; Kimball, B.A.; Nakayama, F.S. The dependence of bare soil albedo on soil water content. *J. Appl. Meteor.* **1974**, *14*, 109–113.
18. Watson, K.; Rowen, L.C.; Offield, T.W. Application of thermal modeling in the geologic interpretation of IR images. *Remote Sens. Environ.* **1971**, *3*, 2017–2041.
19. Price, J.C. Thermal inertia mapping: A new view of the earth. *J. Geophys. Res*. **1977**, *82*, 2582–2590.
20. Xue, Y.; Cracknell, A.P. Advanced thermal inertia modeling. *Int. J. Remote. Sens.* **1995**, *16*, 431–446.
21. Sobrino, J.A.; Kharraz, M.H.; Cuenca, J.; Raissouni, N. Thermal inertia mapping from NOAA-AVHRR data. *Adv. Space Res.* **1998**, *22*, 655–667.
22. Lu, S.; Ju, Z.; Ren, T.; Horton, R. A general approach to estimate soil water content from thermal inertia. *Agric. For. Meteorol*. **2009**, *149*, 1693–1698.
23. Minacapilli, M.; Cammalleri, C.; Ciraolo, G.; D'Asaro, F.; Iovino, M.; Maltese, A. Thermal inertia modeling for soil surface water content estimation: A laboratory experiment. *Soil Sci. Soc. Am.* **2012**, *76*, 92–100.
24. Ulaby, F.T.; Sarabandi, K.; McDonald, K.; Whitt, M.; Dobson, M.C. Michigan microwave canopy scattering model. *Int. J. Remote. Sens.* **1990**, *11*, 1223–1253.
25. Schmugge, T.J.; Blanchard, B.; Anderson, A.; Wang, J. Soil moisture sensing with aircraft observations of the diurnal range of surface temperature. *J. Am. Water Resour. Assoc.* **1978**, *14*, 169–178.
26. Njoku, E.G.; O'Neill, P.E. Multi-frequency microwave radiometer measurements of soil moisture. *IEEE Trans. Geosci. Remote Sens.* **1982**, *220*, 468–475.
27. Shi, Y.-L. Thermal infrared inverse model for component temperatures of mixed pixels. *Int. J. Remote. Sens*. **2011**, *32*, 2297–2309.
28. Wigneron, J.P.; Chanzy, A.; Calvet, J.C.; Bruguier, N. A simple algorithm to retrieve soil moisture and vegetation biomass using passive microwave measurements over crop fields. *Remote Sens. Environ.* **1995**, *51*, 331–341.
29. Stisen, S.; Sandholt, I.; Nørgaard, A.; Fensholt, R.; Jensen, K.H. Combining the triangle method with thermal inertia to estimate regional evapotranspiration—Applied to MSG-SEVIRI data in the Senegal River basin. *Remote Sens. Environ.* **2008**, *112*, 1242–1255.
30. Price, J.C. Using spatial context in satellite data to infer regional scale evapotranspiration. *IEEE Trans. Geosci. Remote Sens*. **1990**, *28*, 940–948.
31. Carlson, T.N. An overview of the "Triangle Method" for estimating surface evapotranspiration and soil moisture from satellite imagery. *Sensors* **2007**, *7*, 1612–1629.
32. Li, Z.-L.; Tang, R.L.; Wan, Z.; Bi, Y.; Zhou, C.; Tang, B.H.; Yan, G.; Zhang, X. A review of current methodologies for regional evapotranspiration estimation from remotely sensed data. *Sensors* **2009**, *9*, 3801–3853.

33. Gillies, R.R.; Carlson, T.N.; Cui, J.; Kustas, W.P.; Humes, K.S. A verification of the "triangle" method for obtaining surface soil water content and energy fluxes from remote measurements of the Normalized Difference Vegetation Index (NDVI) and surface radiant temperature. *Int. J. Remote. Sens.* **1997**, *18*, 3145–3166.
34. Sandholt, I.; Rasmussen, K.; Andersen, J. A simple interpretation of the surface temperature/vegetation index space for assessment of surface moisture status. *Remote Sens. Environ.* **2002**, *79*, 213–224.
35. Tang, R.L.; Li, Z.-L.; Chen, K.S. Validating MODIS-derived land surface evapotranspiration with *in situ* measurements at two AmeriFlux sites in a semiarid region. *J. Geophys. Res.* **2011**, doi:10.1029/2010JD014543.
36. Petropoulos, G.; Carlson, T.N.; Wooster, M.J.; Islam, S. A review of Ts/VI remote sensing based methods for the retrieval of land surface energy fluxes and soil surface moisture. *Prog. Phys. Geog.* **2009**, *33*, 224–250.
37. Carlson, T.N.; Gillies, R.R.; Perry, E.M. A method to make use of thermal infrared temperature and NDVI measurements to infer surface soil water content and fractional vegetation cover. *Remote Sens. Rev.* **1994**, *9*, 161–173.
38. Gillies, R.R.; Carlson, T.N. Thermal remote sensing of surface soil water content with partial vegetation cover for incorporation into climate models. *J. Appl. Meteorol*. **1995**, *34*, 745–756.
39. Moran, M.S.; Clarke, T.R.; Inoue, Y.; Vidal, A. Estimating crop water deficit using the relation of between surface air temperature and spectral vegetation index. *Remote Sens. Environ.* **1994**, *49*, 246–263.
40. Wan, Z.; Wang, P.; Li, X. Using MODIS land surface temperature and Normalized Difference Vegetation Index products for monitoring drought in the Southern Great Plains, USA. *Int. J. Remote. Sens.* **2004**, *25*, 61–72.
41. Patel, N.R.; Anapashsha, R.; Kumar, S.; Saha, S.K.; Dadhwal, V.K. Assessing potential of MODIS derived temperature/vegetation condition index (TVDI) to infer soil moisture status. *Int. J. Remote. Sens.* **2009**, *30*, 23–39.
42. Carlson, T.N.; Gillies, R.R.; Schmugge, T.J. An interpretation of methodologies for indirect measurement of soil water content. *Agric. For. Meteorol*. **1995**, *77*, 191–205.
43. Chen, J.; Wang, C.; Jiang, H.; Mao, L.; Yu, Z. Estimating soil moisture using Temperature-Vegetation Dryness Index (TVDI) in the Huang-huai-hai (HHH) Plain. *Int. J. Remote Sens.* **2011**, *32*, 1165–1177.
44. Nemani, R.; Running, S. Land cover characterization using multi-temporal red, near-IR and thermal-IR data from NOAA/AVHRR. *Ecol. Appl.* **1997**, *7*, 79–90.
45. Clarke, T.R. An empirical approach for detecting crop water stress using multispectral airborne sensors. *HortTechnology* **1997**, *7*, 9–16.
46. Zhao, W.; Jelila, L.; Zhang, X.-Y.; Li, Z.-L. Surface Soil Moisture Estimation from SEVIRI Data Onboard MSG Satellite. In Proceedings of the 2010 IEEE International Geoscience and Remote Sensing Symposium, Honolulu, HI, USA, 25–30 July 2010; pp. 3865–3868.
47. Balsamo, G.; Mahfouf, S.; Bélair, G. A Land Data Assimilation system for soil moisture and temperature: An information content study. *J. Hydrometeorol.* **2007**, *8*, 1225–1242.

48. Glynn, C.; Simon J.; Alice M. Investigating the effects of soil moisture on thermal infrared land surface temperature and emissivity using satellite retrievals and laboratory measurements. *Remote Sens. Environ*. **2010**, *114*, 1480–1493.
49. Tang, R.L.; Li, Z.-L. An application of the Ts-VI triangle method with enhanced edges determination for evapotranspiration estimation from MODIS data in arid and semi-arid regions: Implementation and validation. *Remote Sens. Environ*. **2010**, *114*, 540–551.
50. Zhang, R.H.; Su, H.-B.; Li, Z.-L.; Sun, X.-M.; Tang, X.-Z.; Becker, F. The potential information in the temperature difference between shadow and sunlit of surfaces and a new way of retrieving the soil moisture. *Sci. China Ser. D* **2001**, *44*, 112–123.
51. Zhang, R.H.; Tian, J.; Su, H.B.; Sun, X.M.; Chen, S. Two improvements of an operational two-layer model for terrestrial surface heat flux retrieval. *Sensors* **2008**, *8*, 6165–6187.
52. Long, D.; Singh, V.P. Assessing the impact of end-member selection on the accuracy of satellite-based spatial variability models for actual evapotranspiration estimation. *Water Resour. Res.* **2013**, *49*, 2601–2618.
53. Friedl, M.A.; Davis, F.W. Sources of variation in radiometric surface temperature over a tallgrass prairie. *Remote Sens. Environ.* **1994**, *48*, 1–17.
54. Brutsaert, W. *Evaporation into the Atmosphere: Theory, History, and Applications*; D. Reidel: Dordrecht, The Netherlands, 1982.
55. Land Surface Analysis Satellite Applications Facility. Available online: https://landsaf.meteo.pt/ (accessed on 28 December 2009).
56. Data Hosting Facility of the International Soil Moisture Network. Available online: http://www.ipf.tuwien.ac.at/insitu/ (accessed on 8 January 2013).
57. Monitoring Weather and Climate from Space. Available online: http://www.eumetsat.int/website/home/index.html (accessed on 15 May 2012).
58. Chen, B.X.; Zhang, X.Z.; Tao, J.; Wu, J.S.; Wang, J.S.; Shi, P.L; Zhang, Y.J.; Yu, C.Q. The impact of climate change and anthropogenic activities on alpine grassland over the Qinghai-Tibet Plateau. *Agr. For. Meteorol.* **2014**, *189–190*, 11–18.